Pi2 pulsations driven by ballooning instability

Andreas Keiling[1]

Received 7 October 2011; revised 31 January 2012; accepted 4 February 2012; published 31 March 2012.

[1] With the evidence set forth in this study, we argue that ballooning modes are viable candidates for the generation of high-latitude Pi2 pulsations. In the scenario proposed here, it is the spatial separation ballooning wave perturbations along an energized boundary in the near-Earth plasma sheet combined with a westward ion diamagnetic drift, which imprint a temporal signature, namely, Pi2 pulsation, on conjugate, stationary ground stations. The ballooning wave perturbations are connected via field-aligned currents to the ionosphere causing Pi2 perturbations in the ground magnetic field. The observational evidence for this mechanism was conjugate spacecraft and ground data, showing correlated diamagnetic plasma perturbations and ground magnetic field oscillations, for two spatially separated, simultaneously occurring Pi2 events on 23 March 2007. The plasma perturbations were westward-drifting waves with azimuthal mode number, m, of approximately 40 consistent with drift ballooning modes. During the Pi2 events, particle energy and energy flux gradually increased until the onset of major particle injections, causing auroral intensifications and additional larger-amplitude Pi2s. The ground Pi2s, also shown to be westward-traveling, were superposed on a slowly decreasing H component which abruptly turned into a substorm bay. A ballooning-driven, high-latitude Pi2 differs from a high-latitude Pi2 that starts synchronized with substorm onset and that has been attributed to the transient response mechanism in that it is the frequency of drift ballooning mode in the near-Earth plasma sheet that determines the Pi2 frequency and not the bounce frequency of Alfvén waves along a field line. The geophysical context for this type of Pi2 is a class of substorms that develop from a plasma instability in the near-Earth plasma sheet. If this instability does not lead to a substorm breakup, it could lead to a pseudo-breakup. Hence, it is also likely that some Pi2s associated with pseudo-breakup are caused by the mechanism described here.

Citation: Keiling, A. (2012), Pi2 pulsations driven by ballooning instability, *J. Geophys. Res.*, *117*, A03228, doi:10.1029/2011JA017223.

1. Introduction

[2] Pi2 pulsations (or Pi2s) are brief (approximately 10 min), periodic (40–150 s), ultra-low frequency (ULF) pulsations excited by a source in the nightside magnetosphere. Although Pi2s are best known for their association with substorm onset and we know most about this Pi2 type, they also occur during other magnetospheric modes, such as poleward boundary intensification, pseudo-breakup, and sawtooth-injection events. For example, *Liou et al.* [2000] showed in a statistical study that a significant fraction of Pi2s are not associated with auroral breakup (i.e., substorm). In fact, Pi2s have even been observed during very quiet times [*Sutcliffe*, 1998]. Pseudo-breakups begin like substorms, at least phenomenologically, but they do not reach the same intensity and global scale as full substorms [e.g., *Voronkov et al.*, 2003]. While the physical relationship between pseudo-breakups and substorms has not been determined conclusively, a common phenomenon of both is a Pi2 at onset. Sawtooth injection events are quasiperiodic, intense energy releases accompanied by sawtooth-shaped energetic particle fluxes at geosynchronous orbit [e.g., *Henderson et al.*, 2006]. Although they typically occur during storm intervals, the phenomena associated with a single injection event are similar to those of a substorm, including a Pi2 superimposed on the H bay. In recent years, attention has been given to Pi2s during periods of poleward boundary intensifications [*Sutcliffe and Lyons*, 2002; *Kim et al.*, 2005a; *Keiling et al.*, 2008a], which are auroral intensifications at the poleward boundary of the auroral oval [*Lyons et al.*, 1999].

[3] Among Pi2 models, several of them attempt to explain the generation of high-latitude Pi2s. The most widely accepted model is the transient response model [e.g., *Baumjohann and Glassmeier*, 1984]. The BBF-driven Pi2 model generating inertia current Pi2 [*Kepko et al.*, 2001] and the reconnection-driven Pi2 model [*Keiling et al.*, 2006, 2008a] also deal with high-latitude Pi2s. The paucity of reports for these latter two models makes them still

[1]Space Sciences Laboratory, University of California, Berkeley, California, USA.

0148-0227/12/2011JA017223

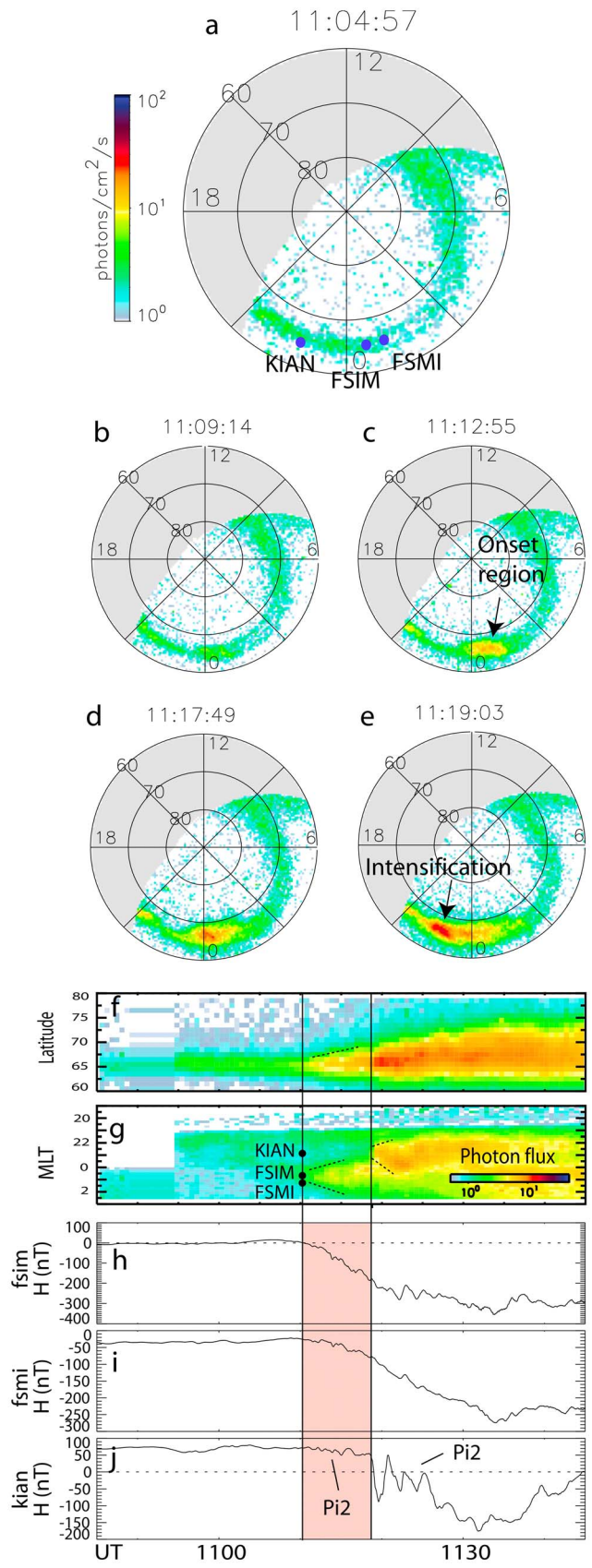

speculative, however. Even the plasmaspheric virtual resonance has been associated with high-latitude Pi2s in the lobe [*Lee*, 1998; *Lee and Kim*, 1999; *Kim et al.*, 2005b]. With the evidence set forth in this study, we argue that ballooning modes in the near-Earth plasma sheet are viable candidates for the generation of high-latitude Pi2 pulsations. We focus on one substorm event (23 March 2007) for which there was ground and space coverage. Results of an earlier study [*Keiling et al.*, 2008c] that investigated this substorm have been incorporated here. This study reported two active regions in the near-Earth plasma sheet that showed plasma perturbations with different periods followed by energetic particle injections at slightly different times. While the authors already suggested that a ballooning mode operated during this substorm, here we investigate its role in generating ground Pi2 by showing additional ground data for two Pi2 events, occurring nearly simultaneously at different locations.

[4] Here we use data from the Time History of Events and Macroscale Interactions during Substorms (THEMIS) mission [*Angelopoulos*, 2008; *Bester et al.*, 2008; *Sibeck and Angelopoulos*, 2008] to describe the Pi2 source region in the near-Earth plasma sheet, using multipoint magnetic field and particle measurements [*Auster et al.*, 2008; *McFadden et al.*, 2008]. The ground Pi2s were analyzed with data from THEMIS's ground magnetometers [*Russell et al.*, 2008], the 210° Magnetic Meridian network (210MM) [*Yumoto et al.*, 1996] and the Geophysical Institute Magnetometer Array (GIMA). Optical data came from THEMIS's all-sky imagers [*Mende et al.*, 2008] and the Polar UVI space imager [*Torr et al.*, 1995].

2. Observations

[5] On 23 March 2007 a substorm with several intensifications occurred. The initial onset, at ~1110 UT, was located post-midnight between 0 and 1 h MLT near the ground stations FSIM and FSMI (Figure 1c). West of this breakup region near KIAN, an auroral intensification occurred between 22 and 23 h MLT about 9 min later (Figure 1e). The spatial and temporal evolution of the aurora is shown in latitude-MLT keograms (Figures 1f and 1g). The first onset region expanded poleward, westward, and eastward (as indicated by dashed lines after the first vertical solid line from the left). At the same time, FSIM and FSMI recorded a typical, negative *H* deflection indicative of substorm expansion. KIAN, located farther west (see dots on the first vertical line indicating the MLT locations of the three ground stations), was not engulfed by the expanding aurora until the auroral intensification (second vertical line from the left in Figures 1g and 1j). Consequently, KIAN initially did not record a strong *H* bay deflection. It did, however, record a small-amplitude Pi2 that appears to be unrelated to the Pi2 associated with the onset region at FSIM and FSMI

Figure 1. Selected in situ, ground magnetometer, and optical data from the 23 March 2007 substorm. (a–e) Several UVI images from the Polar-UVI showing parts of the substorm development. (f and g) Keograms from Polar-UVI and (h–j) ground magnetometer data from the selected ground stations.

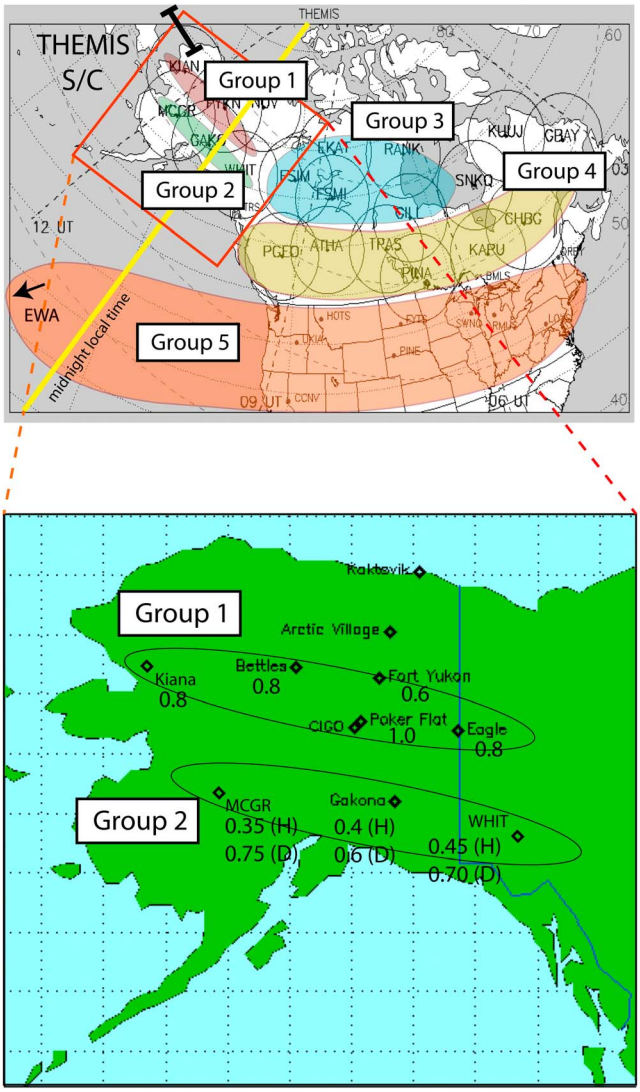

Figure 2. Geographic maps with THEMIS trace (see text for mapping information). Each group is discussed in the text.

(Figure 1j), as further justified below. The auroral intensification expanded westward and eastward (indicated by dashed lines after second line in Figure 1g) but more dominantly eastward. In concert with this expansion, KIAN recorded a very large-amplitude Pi2 (Figure 1j) that was investigated by *Keiling et al.* [2008b].

[6] Here we focus on the first, small-amplitude Pi2 recorded at KIAN with the goal of identifying its generation mechanism. To determine its spatial extent, we inspected magnetometer data from other stations close to and far away from KIAN. These data are described in section 2.1. In section 2.2, spacecraft data from the Pi2 source region in the near-Earth plasma sheet are presented. In addition, we present in section 2.2 ground and space data of a second Pi2 event that occurred during the same time period. This Pi2 was located farther west and had a different waveform than the first. We argue that it was generated by the same mechanism but at a different region in space.

2.1. Ground Observations

[7] During the time of interest (1110–1116 UT), different Pi2s were recorded at low- to high-latitude stations, covering a large area. The ground stations were organized into five groups on the basis of waveform similarities (Figure 2). Group 1 (including KIAN) shows time delayed, coherent Pi2s whose source region was monitored by THEMIS spacecraft (see section 2.2). Group 2 stations are located south of Group 1. Both groups encompass high-latitude stations (>60° magnetic latitude). Group 3, which also comprises high-latitude stations but farther east of the Alaskan stations, shows Pi2s that are less coherent in appearance and are likely associated with the initial substorm onset near FSIM and FSMI (possibly caused by the transient response of the substorm current wedge). We also inspected data from low- and midlatitude stations (<60° magnetic latitude, Groups 4 and 5) outside Alaska, which showed identical Pi2 over a large longitudinal and latitudinal range, likely caused by cavity mode resonance. The observations from low-latitude stations (Group 4) showed no time shifts, whereas those from the midlatitude stations (Group 5) showed an eastward-propagating Pi2. Next we discuss selected Pi2s from each group in more detail.

[8] Figure 3 shows unfiltered and filtered magnetometer data from four Alaskan stations (Group 1). A dual slope in the *H* component with Pi2s superimposed on both slopes can be seen (first slope: 1110–1116 UT; second slope: 1116–1124 UT). The Pi2 of interest is superimposed on the first, shallower slope (red shaded area). The plots at bottom of Figure 3 show filtered (5 s, 100 s) data of this Pi2. The crests and troughs from different stations are correlated with time delays (highlighted by slanted dashed lines) propagating westward from EAGL (Eagle) toward KIAN (Kiana) (see also the locations of the stations marked in the ASI images in Figure 3 (top)). The phase speed of the disturbance is of the order of 50 km/s. In addition, at KIAN the amplitude increases with time (see dashed lines). With the exception of the last pulse (last dashed line on the right), this increase is not apparent at BETT and POKR, and the amplitude variations at EAGL are more erratic.

[9] Figure 3 (top) shows approximate alignment along auroral arc structures of the four ground stations that recorded the Pi2. The ASI images, which were taken at 1112:29 UT, are from cameras installed at KIAN and FYKN. Three additional ground stations at lower latitude are also indicated by yellow dots; their data will be shown later. The bright regions (circled by red lines) were caused by smoke from a nearby factory. Subsequent ASI images reveal that the westward expansion of the initial substorm onset (at ~1110 UT near FSMI and FSIM) reached POKR at ~1114 UT and continued to expand westward (Figures 4a–4d). In contrast, the auroral intensification onset that caused the sharp *H* drop at KIAN around 1118:30 UT occurred west of KIAN (Figure 4c) and expanded eastward (Figure 4d). Before and during the Pi2 event, small undulations and small bright spots (not shown) were seen in the fainter arcs. Their relationship, if any, to the magnetic Pi2 signature is not apparent (see also section 3.2 for additional discussion of the optical signatures).

[10] Figure 5a shows magnetometer data from three Alaskan stations (Group 2: WHIT, GAKO, MCGR) located south of Group 1 stations (compare with Figure 2) and, for

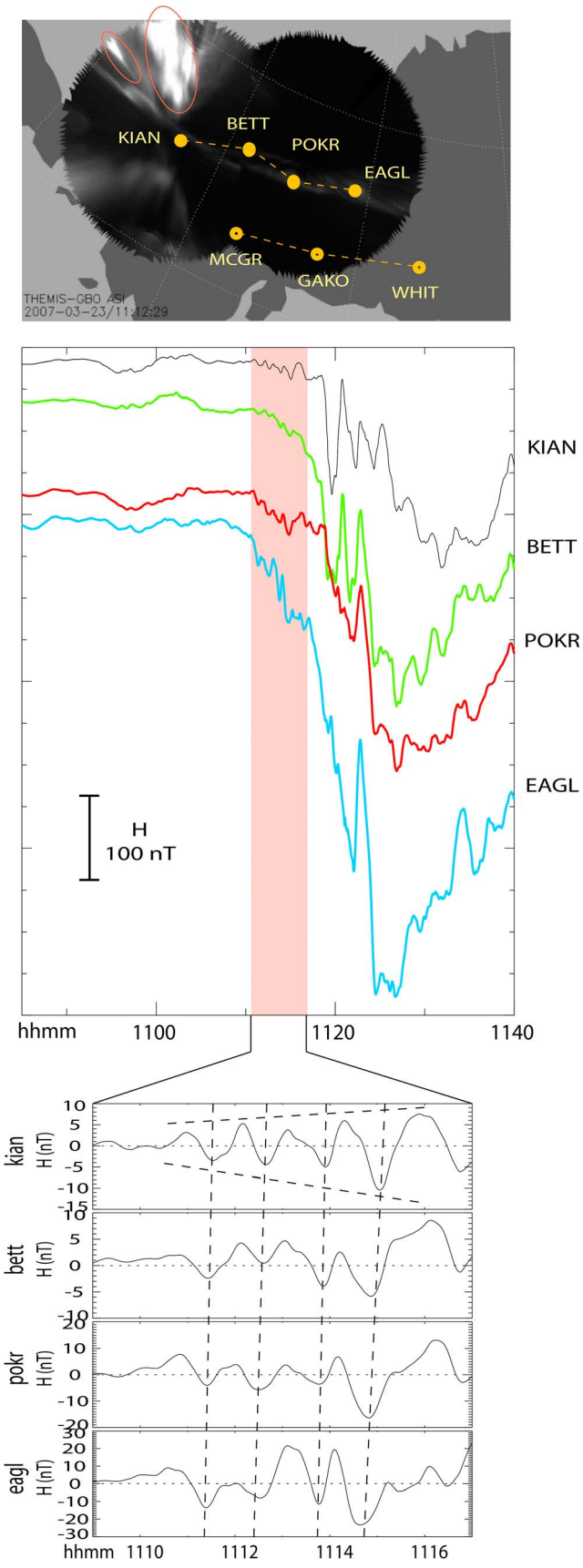

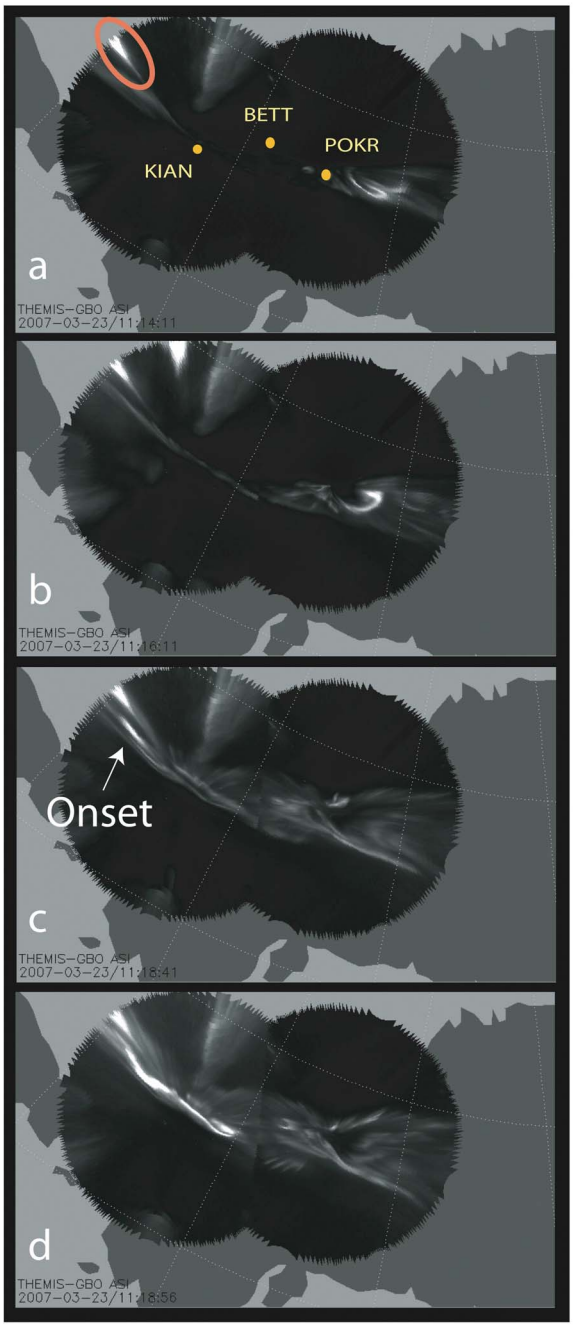

Figure 4. (a–d) A sequence of ASI images during and after the Pi2 event on 23 March 2007. Circled area shows artificial light. The all-sky images are from Kiana (KIAN) and Fort Yukon (FYKN).

Figure 3. Ground magnetometer data (*H* component in nT) from Alaskan ground stations (compare with Figure 2). The shaded red area shows the time period of interest in this study. The plots at bottom show the filtered (5 s, 100 s) data of the Pi2. The ASI images (at top) are from cameras installed at KIAN and FYKN. Seven ground stations are marked by yellow dots. The bright regions, circled by red lines, are smoke light from a nearby factory.

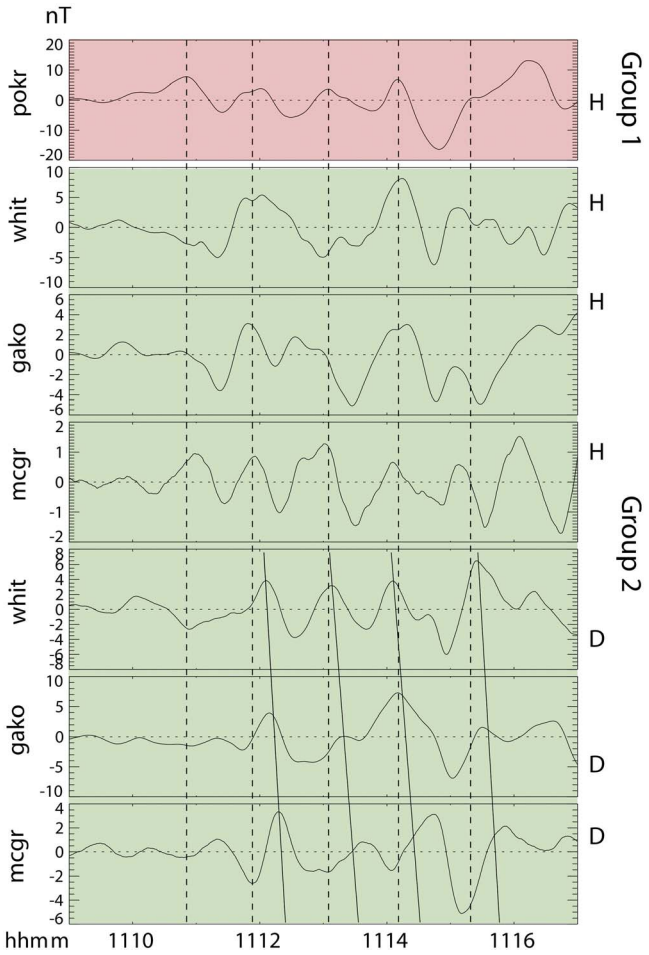

Figure 5a. Ground magnetometer data from selected stations of Group 1 and Group 2 (compare with Figure 2) during the Pi2 event on 23 March 2007.

comparison, data from POKR, which is in Group 1. The *H* and *D* components of Group 2 are shown to determine whether the horizontal electrojet component (related to *H*) or the field-aligned component (related to *D*) shows any similarity with waveforms from Group 1. The waveforms are visually not as similar as they are within Group 1, and there is very little similarity with the waveform at POKR. In addition, we calculated the cross-correlation coefficients of each station's Pi2 (Group 1 and 2) to that of POKR for the time interval 1110–1116 UT. The coefficients are given beneath each station in Figures 2h–2j. Group 1 shows high coefficients, around 0.8. For Group 2, the coefficients are between 0.35 and 0.45 for the *H* component and between 0.6 and 0.75 for the *D* component. This distribution allows for the possibility that the *D* component of Group 2 is related to Group 1. It was noted above that the Pi2 of Group 1 was propagating westward. We drew three slanted lines for the *D* components in Figure 5a that also suggest a westward propagation. The similarity between Groups 1 and 2 is not sufficiently convincing, however, to provide confidence that both observe related Pi2s.

[11] Figure 5b shows comparisons of selected magnetometer data from Groups 1, 3, 4, and 5. Note that data from POKR (Group 1) are unfiltered and filtered (first and second plots, respectively). The filtered POKR data were shifted by 27 s to achieve maximum correspondence with the data from Group 5. First, we compare data from Group 1 with Group 3. Group 3 represents the stations (in particular, FSIM and FSMI) where the first substorm electrojet (onset at ~1110 UT; compare Figure 1) was located and where one would expect large-amplitude, substorm-related Pi2 that have been associated with the transient response model. The Pi2s at FSIM and FSMI, having the largest amplitudes, are similar with signs of westward propagation (time delays between individual signal features), as would be expected for a typical, transient-response Pi2. By comparing crests and troughs, it is

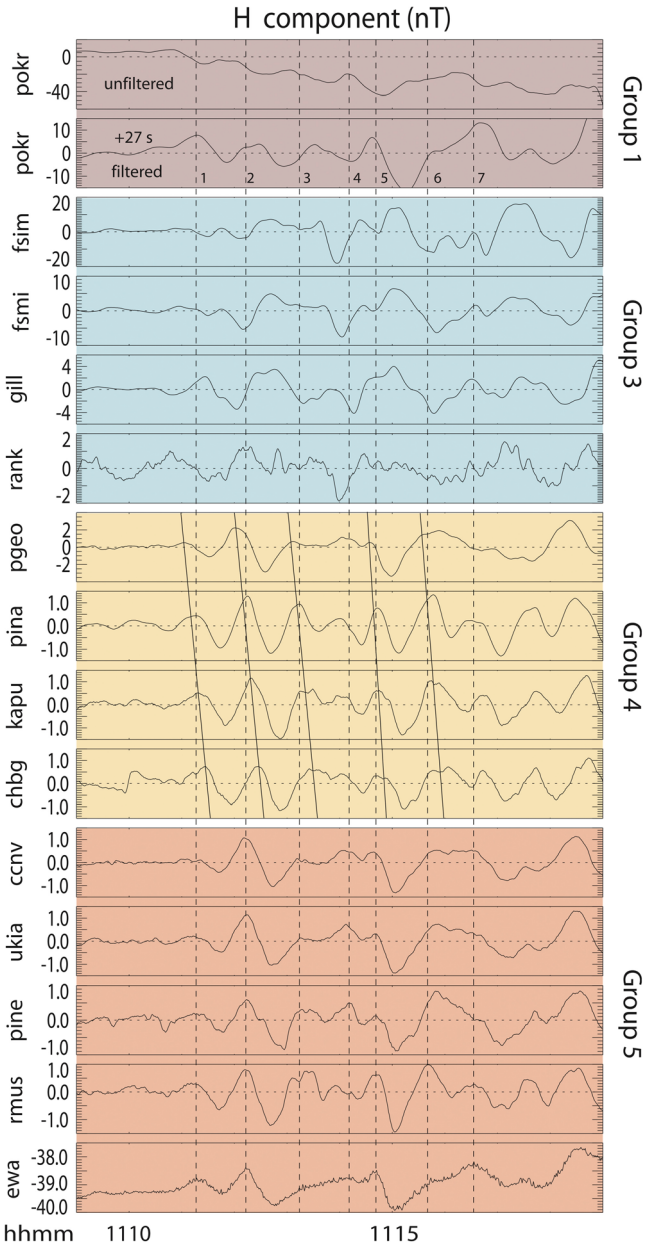

Figure 5b. Ground magnetometer data from selected stations of Group 1, Group 3, Group 4, and Group 5 (compare with Figure 2) during the Pi2 event on 23 March 2007.

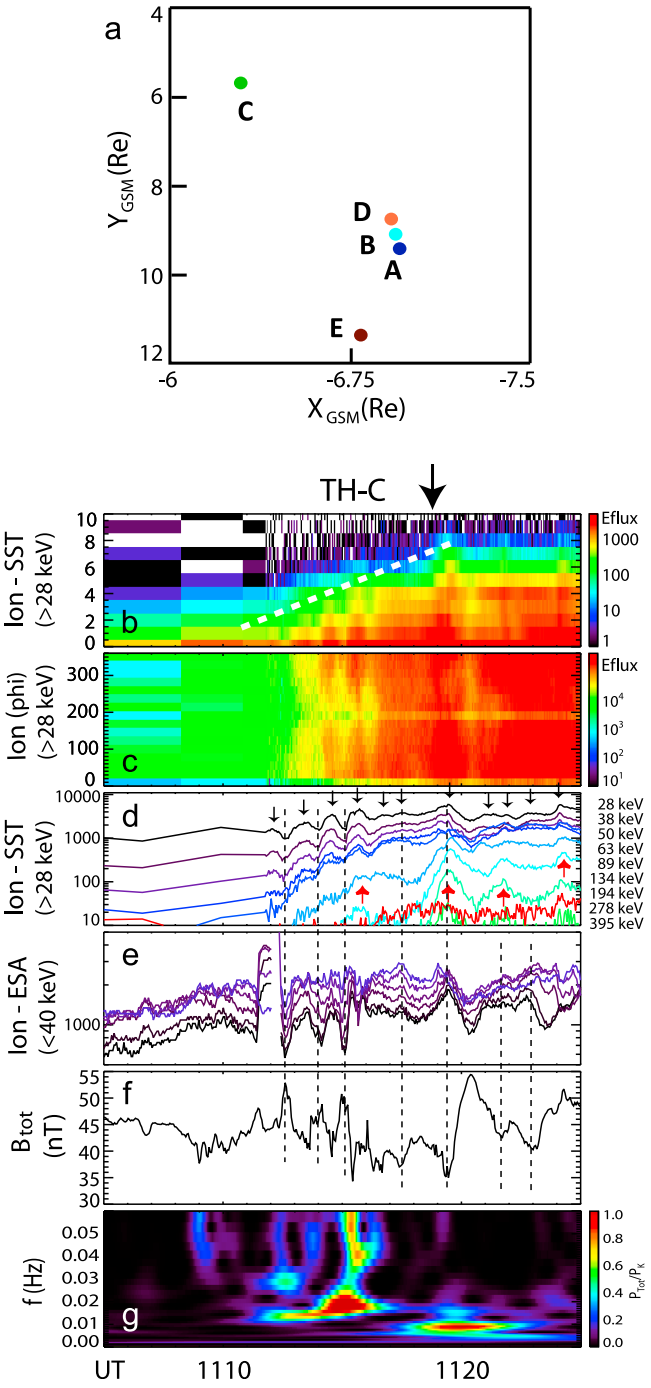

Figure 6. (a) Positions (in R_E) of five THEMIS spacecraft in the X-Y (GSM) plane on 23 March 2007 at 1120 UT. (b–g) Particle and magnetic field data during the 23 March 2007 substorm from THC: ion energy-time spectrogram (Figure 6b); ion azimuth spectrogram as a proxy for pitch angle spectrogram (Figure 6c); ion differential flux covering the energy range from a few eV to 395 keV (Figures 6d and 6e); unfiltered total magnetic field (Figure 6f); the wavelet power spectrum of total B (Figure 6g). Adapted from *Keiling et al.* [2008c].

apparent that the Pi2s in Group 3 are different from the ones in Group 1.

[12] Next, we compare Pi2s from Group 4 with those from Group 5. First, we note that the Pi2 of Group 4 is the same as that of Group 5, as can be seen by comparing the crests at each dashed line (see, for example, PGEO and CCNV). However, whereas the oscillations of Group 5 show almost no time delay among stations separated over many L values from low- to midlatitudes and spanning many hours of local time (compare Figure 2), those of Group 4 show time delays among stations that are aligned longitudinally from east to west at about the same latitude. These time delays indicate an eastward-propagating signal, which is opposite to the propagation direction of the Pi2 in Group 1 (see above). Such westward and eastward propagations are common Pi2 properties [e.g., *Samson*, 1985; *Webster et al.*, 1989]. Because of the global extent of the Group 5 Pi2, we suggest that this Pi2 might originate from a cavity-type mode resonance. A cavity resonance is believed to be excited from a broadband, compressional pulse launched at substorm onset. Therefore, the Group 5 Pi2 and the Pi2 associated with the initial substorm current wedge at 1110 UT (Group 3) are not expected to show the same waveform, which we could confirm. Instead, the onset of the substorm current wedge may have triggered the compressional pulse that led to the cavity resonance at lower latitudes, which is in fact a popular scenario in the literature. Consequently, Group 4 Pi2 must also be part of the cavity resonance. Although the differences with regard to propagation properties of Groups 4 and 5 Pi2s are intriguing, we do not further investigate the generation mechanism for these Pi2s and refer to a future report.

[13] Having established that the Pi2s of Group 4 and Group 5 are related, we now address the question of whether or not the Pi2 of Group 1 is related to those of Groups 4 and 5. Although the Pi2 of, say, POKR (Group 1) resembles those of Groups 4 and 5, there are significant differences, as well: the waveform peaks (e.g., RMUS, CCNV, or PINA) at dashed lines 1, 2, 6, and 7 are nearly coincident; those at lines 3 and 4 are clearly not. A cross-correlation analysis with data from POKR and Group 5 stations (as was performed for POKR and Group 2) shows some surprisingly high coefficients (4–8). However, we caution that Pi2s can have coincidentally high cross-correlation coefficients simply because they must be within the defined Pi2 frequency range. It is also noted that the low-latitude stations show an additional wave cycle (between lines 3 and 4), and thus it is not possible to argue for an additional local auroral current system causing this additional cycle. Therefore, the observed differences rule out a relationship between Group-1 Pi2 and those of Groups 4 and 5.

[14] This view is supported by additional physical arguments. Since the Group-1 Pi2 showed the larger amplitude, it is to be expected that its source was located on a larger L-value shell, i.e., in the outer magnetosphere such as the near-Earth plasma sheet where the substorm current wedge is formed. In this case, an associated transient response of a spawned field-aligned current (FAC) would have had to "force" the Pi2 oscillations onto the lower-latitude cavity resonance, a phenomenon that has never been reported. Note that a cavity mode is an MHD eigenmode that is not periodically driven externally. Moreover, we ruled out that the larger TR-Pi2 of Group 3 was not the driver of the

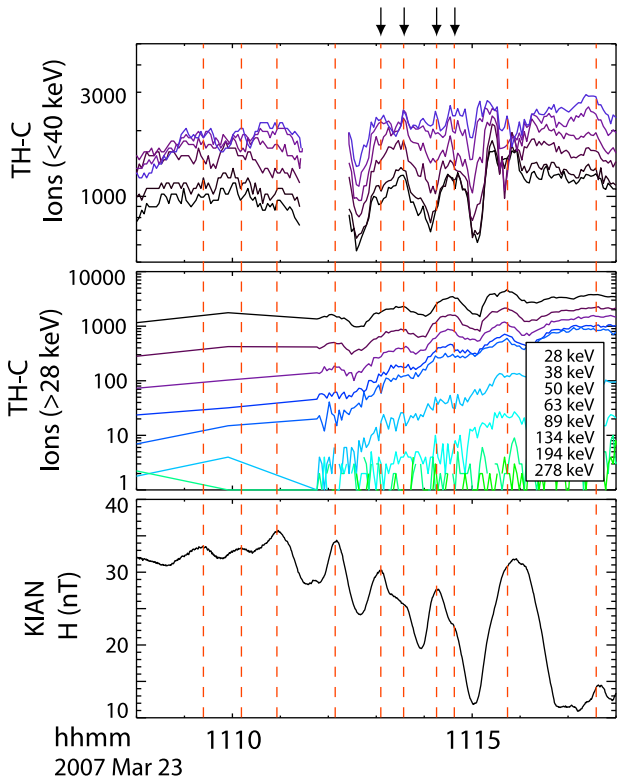

Figure 7. Comparison of ion measurements (energy range from ~keV to >300 keV) at TH-C and ground pulsations during the Pi2 event. Arrows point at additional finer-scale structures (see text for additional explanations).

cavity resonance, and any other smaller FAC would be unlikely to be stronger than the FAC associated with the main substorm that occurred east of Group 1. Hence, it is rather difficult to provide an alternative scenario to explain the similarities and differences among the various groups, if we assumed that Group1 and Group 4/5 showed the same Pi2. In addition, we refer the reader to section 2.2 where a second, independent high-latitude Pi2 is reported, which complicates matters even further.

2.2. Spacecraft Observations and Their Comparison With Ground Observations

[15] At the time of the ground Pi2, the THEMIS fleet was located in the pre-midnight plasma sheet at 8 to 12 R_E (Figure 6). The five spacecraft were in a string-of-pearls configuration, following each other on similar equatorial orbits with an apogee of 15.4 R_E in the following order: TH-C, D, B, A, and E. The spacecraft TH-A, B, and D were closest together (~1000 km); the leading (TH-C) and trailing (TH-E) spacecraft were approximately 2–3 R_E away from other spacecraft in the fleet. According to mapping by *Raeder et al.* [2008], which is based on an MHD simulation, TH-C mapped near KIAN (marked by a black line in Figure 2). The MHD simulation shows significant longitudinal shifts of the spacecraft foot points during different activities. Especially during auroral activity, the footprints are shifted east. Because of mapping uncertainties, it is advisable to check any mapping against actual data on both ends of the field line by finding physical signatures that support the mapping. Since the physical signatures at TH-C and KIAN are very consistent, we find it plausible that the mapping of the MHD simulation is reasonably accurate.

[16] Figure 6 shows magnetic field and particle data from TH-C. The arrow above Figure 6b marks the onset of energetic (>100 keV) ion injections, which are likely causally associated with the auroral intensification [*Keiling et al.*, 2008c]. Here we focus on the interval encompassing the pre-intensification oscillations, from approximately 11:10 UT to 11:17 UT. The energies of the oscillating ions increased up to the intensification onset (white dashed line in Figure 6b). No time delay between different energy channels is visible (compare vertical dashed lines). The dispersionless signature can be explained by periodic entering and leaving of a region of energized plasma. Among other signatures (see below), this periodic entering and leaving can be inferred from the azimuth spectrogram (Figure 6c), which shows that each flux enhancement is associated with a dispersion in azimuth. Owing to the magnetic field and particle sensor orientation, the azimuth is nearly equivalent to the pitch angle during this time interval. The azimuth angles 130° and 310° correspond approximately to the field-aligned and anti-field-aligned directions. Hence, the particles first show perpendicular pitch angles and, only later, field-aligned pitch angles. *Keiling et al.* [2008c] argued that this time period corresponds to the crossing of a horizontally layered boundary. Note that the spacecraft was only partially immersed in the energized boundary layer, as seen in the particles' azimuth which never completely isotropized during the period of interest. An opposite azimuth dispersion indicates a boundary motion in the opposite direction. Figures 6f and 6g show the unfiltered total magnetic field and its wavelet power spectrum, respectively. The magnetic oscillations are out of phase by 180° with the oscillations of the particle flux.

[17] A comparison of in situ measurements with ground magnetometer data reveals one-to-one correlations. Figure 7 shows ion fluxes for different energy channels from TH-C and the *H* component from the high-latitude ground station KIAN (estimated to be closest to the foot point of TH-C). Both waveforms are very similar (i.e., same periodicity). Good one-to-one correlation can also be seen for smaller structures such as the "double peaks" (see arrows), which can be seen on several wave crests. This fine structure gives additional confidence that ground and in situ signals are related. Note the lack of any time delay between ground and space data, which will be further addressed in section 3.

[18] In section 2.1 it was shown that the ground Pi2 at KIAN propagated westward, as inferred from signal time delays at neighboring stations. Therefore, one can ask whether the correlated boundary oscillations propagated westward in space, as well. Ideally, more than one spacecraft is needed for this determination. However, no additional spacecraft was close enough to TH-C to have recorded the same boundary oscillations. Instead, three other THEMIS spacecraft (TH-D, TH-B and TH-A), located approximately 3 R_E farther west of TH-C, were close enough to each other to have recorded similar signals (see below). Hence, we analyzed these data for an interspacecraft comparison and then compared them with near-conjugate ground data that also recorded a Pi2. It is important to note that the oscillation

period and injection onset time recorded by the spacecraft group were different from those at TH-C. Therefore, it is apparent that the spacecraft group was immersed in a different active region of the near-Earth plasma sheet than TH-C. In other words, at least two active regions existed simultaneously and were monitored by different THEMIS spacecraft [see also *Keiling et al.*, 2008c].

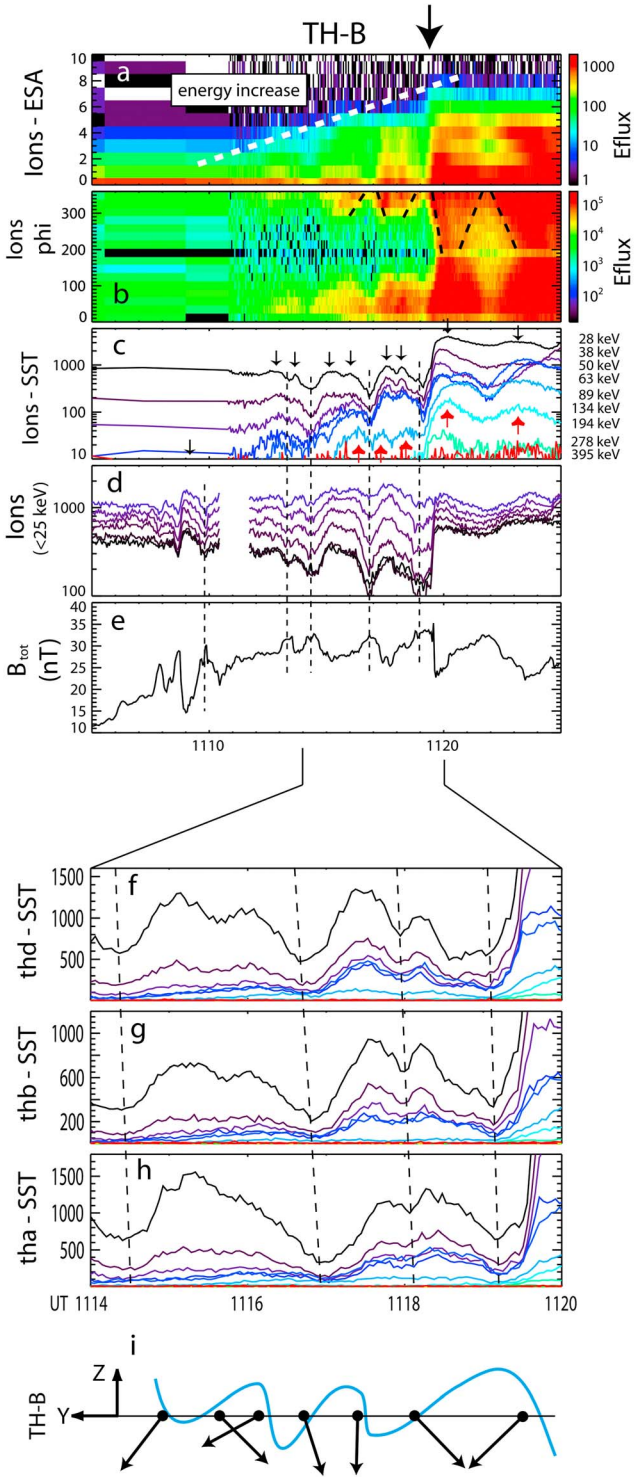

[19] Figures 8a–8e show data from TH-B in a format similar to that of Figure 6. Particle and magnetic field oscillations between 1110 UT and 1120 UT, followed by an energetic ion injection (arrow above Figure 8a), can be identified. Figures 8f–8g show ion fluxes from the three spacecraft for comparison. The time delays from TH-D to TH-B and to TH-A indicate westward propagation of the signal (see spacecraft locations in Figure 6a) with an upper speed limit of 230–280 km/s. The three spacecraft were located ~0.6 R_E below the nominal neutral sheet along an approximate line. As shown by *Keiling et al.* [2008c], the flux modulations were caused by the spacecraft's periodic entering into energized plasma. The time delays show that the energized plasma was first entered and first exited by the same spacecraft rather than first entered and last exited by the same spacecraft. This pattern suggests that the particle and field perturbations correspond to bulges in the boundary of the energized plasma moving past the spacecraft. This scenario was confirmed by minimum variance analysis (MVA) applied to separate time intervals that correspond to entering into (decreasing |Bx|) and exiting from (increasing |Bx|) the energized plasma. Determined MVA directions, which correspond to the normal direction of the moving boundary perturbations, are shown at the bottom of Figure 8 as projections onto the Y-Z (GSM) plane. The alternating directions of the normal vector in the +Y and −Y directions due to the passing of several boundary perturbations (i.e., boundary waves) are schematically illustrated by the wavy blue line.

[20] The spacecraft group (TH-D, TH-B, TH-A) was not conjugate to KIAN, as was TH-C, but were located farther west. It appears that the closest stations to conjugate field lines were TIK or ZYK from the 210°MM magnetometer array, although we believe that the foot points were farther away from these stations than the ground-space conjunction between KIAN and THC. Figure 9 compares space data and ground data from ZYK, which shows the best correspondence. It is again the time period (shaded red) before the energetic plasma injections at ~1120 UT that is of interest. We find good correspondence between both signals after the waveform of ZYK was shifted by +30 s, which means that the ground oscillations were recorded before the space oscillations. We emphasize that the period and waveform in Figure 9 differ significantly from those recorded at KIAN (Figure 8); that is, this ground Pi2 must have a different source.

Figure 8. (a–e) Particle and magnetic field data during the 23 March 2007 substorm from TH-B: ion energy-time spectrogram (Figure 8a); ion azimuth spectrogram as a proxy for pitch angle spectrogram (Figure 8b); ion differential flux covering the energy range from a few eV to 395 keV (Figures 8c and 8d); unfiltered total magnetic field (Figure 8e). (f–i) Boundary analysis for the three closely spaced THEMIS spacecraft: ion energy flux for individual energy channels (Figures 8f, 8g, and 8h); projections of the MVA directions onto the Y-Z (GSM) plane for TH-B (Figure 8i). The blue wavy line in Figure 8i schematically illustrates the perturbations on the boundary. Adapted from *Keiling et al.* [2008c].

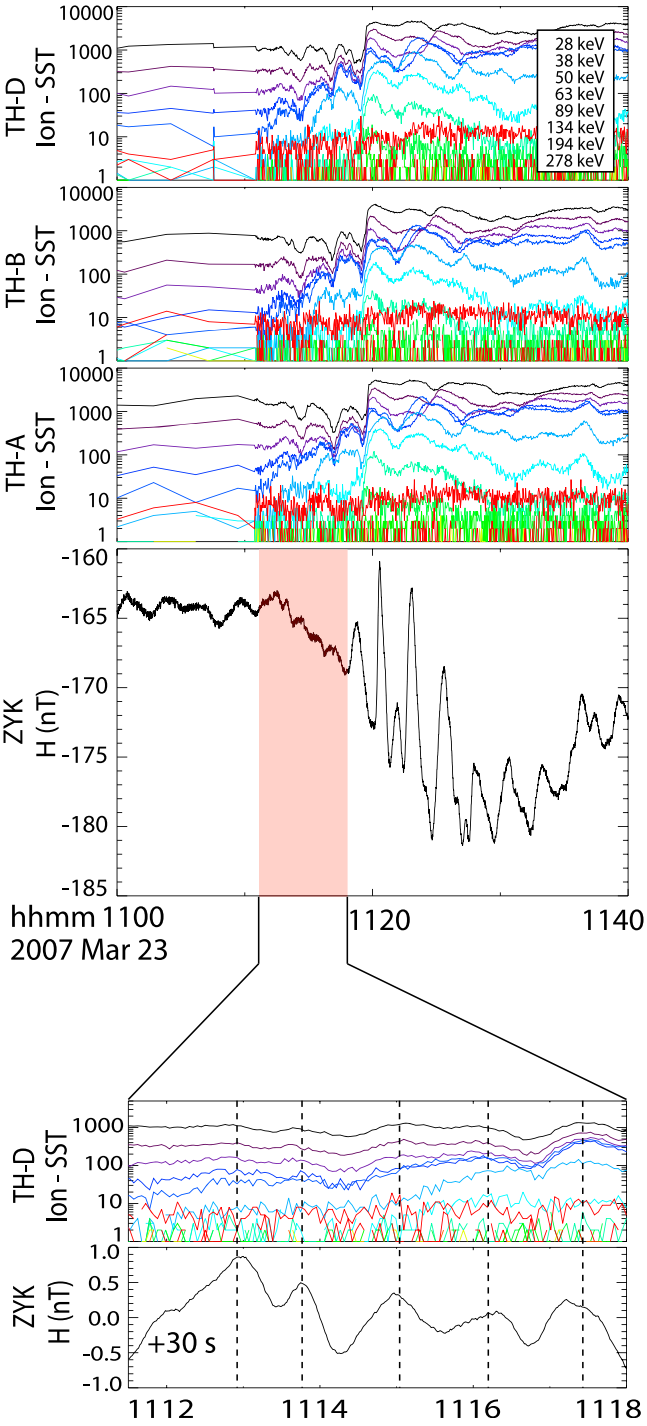

Figure 9. Comparison of ion flux enhancements (at TH-B, TH-D, and TH-A) and magnetic field pulsations at ZYK (ground station of the 210MM network; 65.75° latitude and 150.78° longitude geographic) for the time interval marked by the red shaded region in the fourth plot from the top. Similar fine structure is highlighted by dashed lines in the bottom two plots.

[21] In summary, these ground-space observations and comparisons demonstrate the existence of two active regions, executing different oscillations, in the near-Earth plasma sheet separated by approximately 3 R_E. Both space regions appear to be causally connected to different ground Pi2s at high latitudes as inferred from the excellent correspondence between waveforms from ground and space data.

3. Discussion

[22] In section 2 we presented ground and space data for two Pi2 events that preceded an auroral breakup. In this section we propose the following scenario for their generation. First, an auroral onset occurred over Canada near FSIM and FSMI, spawning a substorm current wedge and an associated Pi2 in the vicinity of the high-latitude substorm electrojet. The disturbance in the near-Earth plasma sheet also launched a compressional pulse that triggered a global cavity mode resonance at low and middle latitudes. During the substorm expansion phase, two localized space regions (9–12 R_E geocentric distance) west of the onset regions were independently active, developing ballooning mode oscillations with different periods, followed by energetic ion injections and additional auroral intensifications. The pre-intensification ballooning mode oscillations were coupled to the ionosphere, causing two separate high-latitude Pi2s. Figure 10 schematically shows the different types of Pi2s that were simultaneously present. The focus of this study is the ballooning-mode-driven Pi2 (BM-Pi2). In sections 3.1–3.5 we will discuss several aspects of the BM-Pi2 generation mechanism.

3.1. Ground-Space Correspondence

[23] The comparison between ground and space data yielded the following features:

[24] 1. One Pi2 was observed at four high-latitude, azimuthally aligned ground stations (EAGL, POKR, BETT, and KIAN). At each station, the Pi2 was time delayed such that it traveled westward at ~50 km/s, which is within the

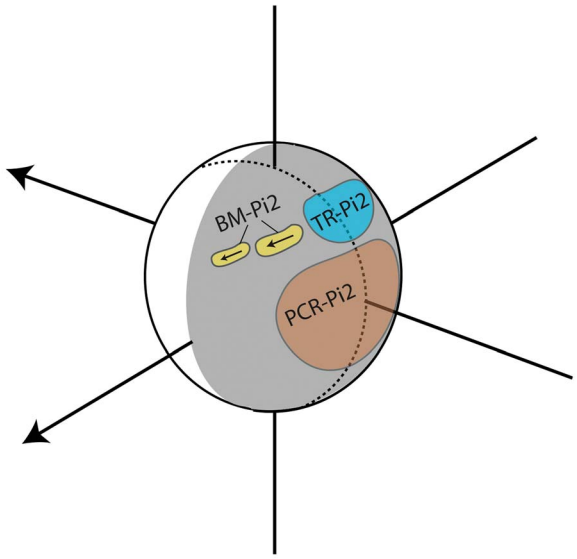

Figure 10. Illustration of various Pi2s which were simultaneously present on 23 March 2007: TR-Pi2 (transient response Pi2), PCR-Pi2 (plasmaspheric cavity resonance Pi2), BM-Pi2 (ballooning mode Pi2). The arrows indicate westward propagation.

velocity range of previous reports [e.g., *Samson*, 1985; *Webster et al.*, 1989]. Simultaneous spacecraft data (TH-C) showed one-to-one correlated, diamagnetic plasma perturbations (out of phase with the total magnetic field), including small-scale features, in the near-Earth plasma sheet. The four ground stations were aligned approximately along an auroral arc that was later immersed in an auroral breakup. Ground stations immediately to the south (WHIT, GAKO, and MCGR) showed coherent correlations in the *D* component, whose waves also propagated westward.

[25] 2. Located west of TH-C, a group of spacecraft (TH-A, TH-B, and TH-D), aligned in a string-of-pearls configuration along their trajectory, recorded diamagnetic plasma perturbations that were one-to-one correlated with a second Pi2. Located at a slightly larger geocentric distance than TH-C, the oscillation period was longer than that at TH-C. The ground Pi2 occurred 30 s before the plasma perturbations. Using the azimuthally aligned spacecraft, it was shown that the plasma perturbations propagated westward with a propagation speed of <280 km/s (upper limit).

[26] 3. The observed one-to-one correlations (including smaller-scale features) between plasma perturbations in the near-Earth plasma sheet and both ground Pi2 events suggest that the ground Pi2s were indeed driven by the plasma perturbations. These plasma perturbations are suggested to be ballooning mode oscillations, as will be further discussed in section 3.2 (see also sections 3.5 and 3.6).

[27] 4. At the time of the high-latitude Pi2s under investigation, additional Pi2s were recorded farther east (high-latitude stations, Group 3) and south (mid- and low-latitude stations, Groups 4 and 5). Cross-correlation analyses and visual inspections suggest that these Pi2s were caused by other sources. Group 3 showed large-amplitude Pi2 with different waveforms/period than Group 1. The Group-3 Pi2 occurred in the vicinity of the initial substorm onset region and was likely associated with the substorm current wedge. Groups 4 and 5 showed identical Pi2s over many hours of local time, reminiscent of a global cavity mode. Although there was some similarity between the Group 4/5 Pi2 and the Group 1 Pi2, we concluded that they were different based on visual inspections and physical arguments.

3.2. Association With Ballooning Mode

[28] Several features of wave activity surrounding substorm onset have been identified (see reviews by *Lui* [1996] and *Ohtani* [2001]). In the late 1980s, it was recognized that substorm onsets are associated with large-amplitude magnetic field fluctuations in the near-Earth plasma sheet [e.g., *Takahashi et al.*, 1987]. *Lui et al.* [1991] interpreted these fluctuations as temporal structures, as opposed to the erratic crossing of a spatial structure (e.g., X line). The magnetic fluctuations encompass low- to high-frequency components [e.g., *Lui and Najmi*, 1997]. High-frequency components have been associated with the mechanism disrupting the current sheet [*Lui et al.*, 1991], while low-frequency components are possibly associated with an MHD instability [e.g., *Miura et al.*, 1989; *Roux et al.*, 1991; *Cheng*, 1991; *Ohtani and Tamao*, 1993; *Bhattacharjee et al.*, 1998; *Cheng and Lui*, 1998] that might pre-condition the current sheet leading to its subsequent disruption.

[29] Recently, Geotail spacecraft observations have provided observational evidence for the drift ballooning mode near the magnetic equator (10 to 13 R_E geocentric distance) a few minutes before dipolarization onset [*Saito et al.*, 2008]. Oscillation periods and wavelengths for several events were estimated to be in the range from 50 to 75 s and up to 7000 km, respectively. In agreement with these observations, we found westward-moving perturbations/wave of an energized plasma boundary with a drift velocity of 230–280 km/s as an upper limit, using three azimuthally aligned THEMIS spacecraft [*Keiling et al.*, 2008c]. The actual velocity of the wavefront could not be determined because of the 1-D-like spacecraft alignment. Velocity and period allow us to estimate the azimuthal mode number, m, of the boundary perturbations. If we assume a speed of, say, 150 km/s for the 60-s period wave, we obtain a wavelength of 9,000 km in the equatorial plane, which corresponds to m = 40. Such large values are expected for ballooning modes [e.g., *Miura et al.*, 1989]. *Keiling et al.* [2008c] also showed that the magnetic oscillations were not correlated with the velocity in agreement with ballooning mode [e.g., *Roux et al.*, 1991; *Saito et al.*, 2008].

[30] Another observational parameter for ballooning instability is the plasma β (particle pressure divided by magnetic pressure). Various studies incorporating different physical effects have derived different instability thresholds, however. *Ohtani and Tamao* [1993] argued that high β is not favorable for the ballooning instability and derived a β of 2 as an upper threshold. Others derived a β—under which ballooning could occur—in the 1 to 10 range [*Liu*, 1997], greater than 16 [*Pritchett and Coroniti*, 1999], and greater than 50 [*Cheng and Lui*, 1998]. These results show that the theoretical picture of ballooning instability in the magnetotail is far from conclusive. If we determine β during the Pi2 of interest here, we find a value of approximately 1 (not shown). However, as inferred from the finite magnetic field, the spacecraft were located significantly away from the equatorial plane, skimming a boundary of energetic particles. The particle energy flux of the boundary perturbations increased throughout the Pi2 activity, suggesting that the perturbations grew and therefore the spacecraft penetrated deeper into the layer of increasingly energized plasma. Such perturbation growth would be expected for the ballooning instability. In this situation, the measured β does not correspond to that of the actual trigger region of the instability, and no immediate conclusion can be drawn from it. If we project β to the equatorial plane, a value of 10 or larger could be expected, which is consistent with ballooning instability (see references above). In comparison, *Saito et al.* [2008] reported a β of greater than 20 for their events, albeit the spacecraft were much closer to the equatorial plane.

[31] Of relevance for the Pi2 generation mechanism proposed here is that two space regions executed diamagnetic plasma perturbations with different periods. These observations suggest that the near-Earth plasma sheet can simultaneously support several ballooning unstable regions [*Keiling et al.*, 2008c] or filamentary structures [*Schindler and Ness*, 1972]. It is also notable that the space region located at a larger radial distance recorded a longer oscillation period. The larger radial distance implies a larger local cross-section of the current sheet layer and/or slightly different physical conditions, which could account for the longer period of ballooning mode oscillations and also a longer wavelength of the drifting mode, although the latter could not be verified

because of lack of additional spacecraft. Each space region caused a high-latitude Pi2. Hence, the ballooning-driven Pi2 scenario can explain the simultaneous occurrence of variable Pi2 periods at high latitudes.

[32] One Pi2 event was recorded at ground stations located approximately along a faint auroral arc. At the end of the Pi2 time interval, the arc region showed an auroral intensification. Therefore, one can conclude that the ground Pi2 was magnetically connected (or close) to the unstable region in the magnetotail that caused the auroral intensification. Such unstable space regions are presumed to be initially very localized in space, which is consistent with the localization of the ground Pi2; only later instability leads to a more widespread reconfiguration of the magnetotail. At auroral intensification, the spacecraft recorded energetic particle injections of the type associated with dipolarizations. This sequence of events suggests that the pre-breakup Pi2 might have been causally related to the auroral intensification and the injections. In an earlier study, *Solovyev et al.* [2000] suggested that high-latitude Pi2s might be associated with the brightening and spatial distortion of auroral arcs rather than with the substorm current wedge (as is the case for the transient response Pi2). Although an auroral arc was present in our event, it was not possible to identify undulations and brightening similar to those reported by *Solovyev et al.* [2000]. *Keiling et al.* [2008c] reported several bead-like auroral structures separated by approximately 0.4 h local time, which would correspond to an azimuthal mode number of 60, a number approximately consistent with m = 40 as inferred from the spacecraft. These beads were recorded in the ultraviolet images, however. The ASI images shown here were taken in the visible spectrum, and it was not possible to convincingly verify the beads in these images. Thus, it is not certain whether the optical signature was related to the ground Pi2 reported here.

[33] In summary, our observations support the occurrence of the drift ballooning mode, and the good correlation between space and ground oscillations suggest that the ground Pi2s were driven by this mode. The drift ballooning mode has a real frequency, which is due to the ion diamagnetic drift [e.g., *Miura*, 2004]. The wavelength (or azimuthal mode number), being a fundamental property of drift ballooning mode, is controlled, among other quantities, by the pressure gradient scale length and the curvature radius. If we apply this scenario to the Pi2 generation, the period, T, of the Pi2 pulsations is then determined by $T = \lambda_{\perp}/V_{ph}$, where $\lambda_{\perp}$ is the perpendicular wavelength of the ballooning mode wave and V_{ph} is its phase velocity. Due to their westward propagation, the wave perturbations are recorded as oscillations at a fixed point in space. This is what the THEMIS spacecraft, which can be considered stationary in the passing wave, recorded. We note that depending on the wavelength and phase speed of the ballooning mode, the Pi2 period will vary and might for other events even lie outside the characteristic Pi2 period range.

3.3. Pi2 Propagation to the Ground

[34] It is notoriously difficult to identify the propagation path of Pi2 signals from the source to the ground. Before reaching ground, the Pi2 signal can convert into other propagation modes, and there have been too few spacecraft to verify such mode conversions. Therefore, many proposed propagation models in the literature are speculative. Our observations also lack the global space coverage to be conclusive. Nevertheless, we propose a scenario that incorporates the unusual feature that the ground Pi2 can occur before the space Pi2. For this discussion we will assume that ballooning instability was the Pi2 generation mechanism as argued in Section 3.2.

[35] Wave perturbations in the near-Earth plasma sheet lead to excess electrons on one side of the wave crests [see *Roux et al.*, 1991, Figure 10]. Streaming of these electrons toward the ionosphere results in an upward field-aligned current. Through the ionosphere, the current connects to the downward current (i.e., the return current), which is connected to the excess positive charge in the wave perturbation in space. Together with the westward drift, the multiple currents are recorded as magnetic oscillations on the ground (Figure 11). The direction of the magnetic deflection observed on the ground (H component) is consistent with the direction of the current flowing from the space perturbations. The growing perturbations in space are thus generators ($\mathbf{E}\cdot\mathbf{j} < 0$) and the ionosphere is the load. Because the ground stations are stationary relative to the drift, they record the currents with the same period as the waves observed by a single spacecraft (which can also be considered stationary in the passing wave). In this coupling scenario, the time delay between space and ground oscillations depends not only on the signal travel time from space to ground, but also on the longitudinal separation between spacecraft and ground stations. Therefore, it should be possible to record a ground Pi2 before a space Pi2 in certain situations (other Pi2 models typically require the opposite). This was indeed the case. Whereas KIAN and TH-C, both nearly magnetically conjugate, recorded the Pi2 at nearly the same time, the Pi2 at POKR occurred before the space Pi2.

[36] In this propagation scenario (Figure 11), the entire current system drifts westward, as does the ballooning mode wave. Whereas the horizontal ionospheric currents cause the H component perturbation (as recorded by EAGL, POKR, BETT, and KIAN), the connecting field-aligned currents could possibly cause perturbations in the D component. Stations located south of these four stations recorded such D component perturbations. It is important to note that waves with high azimuthal wave numbers, as those associated with the ballooning modes, are prone to significant attenuation if they propagate through the ionosphere. In our scenario, however, waves do not propagate from the source (the ballooning instability region); instead, FACs are guided along magnetic field lines into the ionosphere from where the MHD waves could be launched. In fact, high-m azimuthal auroral structures [e.g., *Elphinstone et al.*, 1995] show the existence of FACs with narrow azimuthal separation in the ionosphere.

[37] Furthermore, whereas on the ground the longitudinal propagation speed was ~50 km/s, in space it was less than 280 km/s (exact value is not available). In a statistical study of high-latitude Pi2s, *Uozumi et al.* [2004] reported westward propagations of the order of 70–90 km/s on the ground and a projected velocity of ~500 km/s in the equatorial plane at a location similar to that of our event. Their estimate is close to our measurements, allowing for a smaller ground speed. In general, we remark that it has been challenging for the Pi2 community to explain the large longitudinal propagation

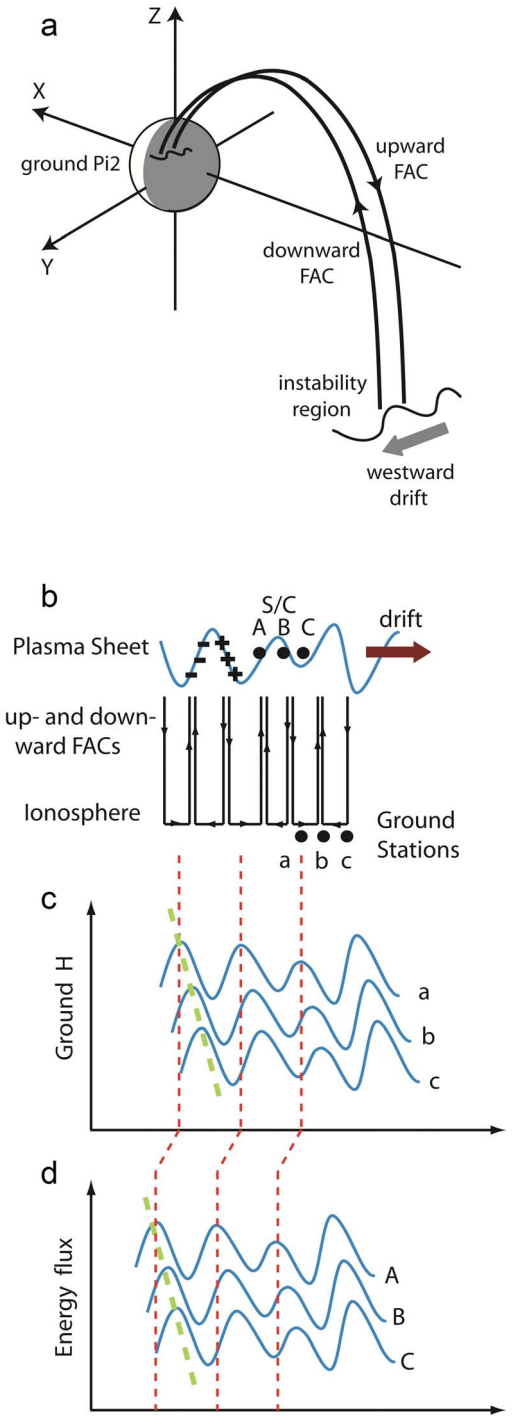

Figure 11. (a) Illustration of the connection of a ground Pi2 and its source region in the magnetosphere. Downward and upward FACs are only shown for one wave pulse. (b) Schematic of perturbations in the near-Earth plasma sheet and the currents leading from the perturbations into the ionosphere. (c) Ground signature recorded at three longitudinally separated ground stations due to FACs from perturbations in space. (d) Plasma perturbations recorded in situ by three azimuthally separated spacecraft.

speeds of ground Pi2s, and no conclusive answer has yet been given. Two different scenarios for the longitudinal Pi2 propagation are reviewed by *Webster et al.* [1989].

3.4. Geophysical Context

[38] A notable feature during the Pi2s reported here (although more pronounced for the first Pi2 event) was the dual slope in the ground *H* component during the substorm. The Pi2 was superposed on the shallower, negative slope of *H*, which was followed by a steeper and longer slope associated with the main injection event and another larger-amplitude Pi2. *Henderson* [2009], for example, reported a dual-slope *H* component in association with a plasma-instability-driven substorm. A shallow slope is also associated with pseudo-breakups (or small substorms) that recover before they steepen and reach large negative values of *H*. Hence it might be that this type of geomagnetic disturbance generates the Pi2 type described here.

[39] The significance of pre-onset oscillations was also reported by, for example, *Ohtani et al.* [1992], who identified a magnetic field perturbation immediately preceding (by ~30 s) substorm onset that grew "explosive"-like, and the authors argued that it may be critical in triggering substorm onset. *Cheng and Lui* [1998] expanded their analysis by arguing that a low-frequency instability in the Pi2 range was excited ~2 min before onset, which led into this explosive growth. *Erickson et al.* [2000] reported quasi-electrostatic oscillations during the growth phase and before onset, calling them trigger waves, and also suggested that these oscillations play a role in triggering the main onset. More recently, *Saito et al.* [2008] and *Liang et al.* [2009] showed pre-onset wave activity in the Pi2 range that was consistent with drift ballooning modes. While these studies reported wave activity in the Pi2-frequency band in the near-Earth plasma sheet, a relationship with ground Pi2 pulsations was not investigated.

3.5. Previous Work on Plasma-Instability-Driven Pi2s

[40] In the past, few studies considered the possibility that plasma instabilities in the near-Earth plasma sheet could generate ground Pi2. *Solovyev et al.* [2000] suggested that the excitation of high-latitude Pi2 during pseudo-breakups and substorm expansion phases, and the spatial distortion of auroral arcs are caused by a common process—namely, a plasma instability in the magnetotail. The authors compared ground magnetometer data to auroral data from all-sky cameras. It was found that the maximum Pi2 amplitude is observed at the same latitude as the auroral arc, and the arc shows wave-like structures. The Pi2 period was found to be consistent with the period of arc oscillation (30–200 s). Hence, it was suggested that temporal wavelets are launched from ripples on the inner plasma sheet boundary. In this scenario, it is assumed that an Alfvén wave is reflected only once from the ionosphere, and the Pi2 is a sequence of wavelets with Pi2 periodicity, presumably launched at different times in the magnetotail. However, although similar periods were reported in the two types of signals (magnetic field and optical), they were not shown to correlate one-to-one, and no spacecraft data were presented to substantiate the model.

[41] Using both ground data and spacecraft data, *Keiling et al.* [2008b] reported correlations among ground Pi2,

auroral modulations, and energetic particle injections in the near-Earth plasma sheet, all of which oscillated with a period of 135 s. The most striking features were the very large ground magnetic field amplitude (δH = 150 nT) and the short (6 s) time delay between the periodic dispersionless ion injections and the ground Pi2. It was speculated that a common source that controlled the periodicity was an oscillatory, non-propagating plasma instability which led to periodic disruptions of the plasma sheet followed by periodic particle injections and ground Pi2. This scenario is not the same as described here, which is a propagating instability. Because of the very large amplitude of the high-latitude Pi2, it was further argued that the individual "Pi2 pulses" were a series of individual ground intensifications, and as such, each pulse would be associated with a near-Earth ion injection.

[42] Finally, we caution the reader not to confuse our scenario with the following, which has a plasma instability as substorm trigger but not as the Pi2 generation mechanism. It has been proposed that a plasma instability can lead to a disruption of the cross-tail current, which in turn can lead to the formation of a substorm current wedge (see review by *Lui* [1996]). Associated with the substorm current wedge are transient Alfvén waves that have been postulated to bounce back and forth until equilibrium has been reached. This "ringing" of flux tubes causes one type of substorm-related Pi2s, the so-called transient response (TR) model (see review by *Baumjohann and Glassmeier* [1984]). In the TR model, the initiator of the substorm current wedge is irrelevant. The characteristic Pi2 frequency is controlled by the length of the travel path along the magnetic field and the speed of the Alfvén wave. The important difference to the Pi2 mechanism proposed here is that in our scenario the wave period of the drift ballooning mode controls the Pi2 period.

4. Conclusions

[43] Here we argued that drift ballooning mode waves in the near-Earth plasma sheet can be the generation mechanism of some high-latitude Pi2s. In general, the ballooning mode is proposed to be initiated in the near-Earth plasma sheet around 9 to 12 R_E. This space region magnetically maps into the high-latitude region on Earth (>60° magnetic latitude), and thus, the ballooning-driven Pi2 model can generate high-latitude Pi2s along conjugate magnetic field lines. It is, however, possible that lower latitude Pi2s are also generated via additional propagation paths.

[44] The ballooning-driven Pi2 is different from the high-latitude Pi2 that starts synchronized with substorm onset and that has been attributed to the TR model. The Pi2 type reported here occurred before auroral breakup in an interval of slow decrease in the geomagnetic H component followed by the steeper substorm bay. It is not the bouncing nature of the currents that controls the Pi2 periodicity, as for the TR model, but the period of drift ballooning mode oscillations in the near-Earth plasma sheet. For the event on 23 March 2007, we presented one-to-one correlations of plasma perturbations, which we argued to be drift ballooning waves in the near-Earth plasma sheet, and ground magnetometer data. It was shown that two space regions were simultaneously ballooning-active, each causing different high-latitude Pi2s. Hence, the ballooning-driven Pi2 scenario can explain variable, simultaneous Pi2 periods at high latitude. An unusual observation was that the Pi2 in space and on the ground occurred in reversed temporal order to what is typically expected, which might be a signature that helps to separate the ballooning-driven Pi2 from other Pi2 types.

[45] A common challenge in Pi2 research is to provide convincing evidence to connect the source region with the ground via different propagation modes because of the still rather limited number of spacecraft in key regions. We provided an explanation that was based on westward drifting field-aligned currents flowing between the instability region and the ionosphere. Although the observational evidence for the ballooning mode has been increasing in the last decade, the mode's coupling to the ground/ionosphere is far from being understood. In particular, the coupling via field-aligned currents might affect the dynamics of the ballooning mode itself [*Pritchett and Coroniti*, 1999]. It is beyond the scope of this paper to determine the exact type of drift ballooning mode that generates the new type of Pi2 proposed here.

[46] Although the idea of plasma instability as a Pi2 generation mechanism has occasionally been mentioned in the literature, satisfactory evidence had not been provided. Here we add to the ongoing investigation of identifying and characterizing a plasma-instability-driven Pi2 model. To our knowledge, our event study provides the first observational evidence for an association between drift ballooning waves and ground Pi2. One complication was that this substorm event showed several intensifications and several Pi2s with different properties over many hours of local time and many latitudes, which resulted in complex signatures. Thus, criticism could arise regarding the separation of the several activities. However, such a complex scenario shows that different Pi2s can be present simultaneously. Naturally, Pi2s that show more typical properties and are isolated from other phenomena were investigated first by researchers. However, we also need to understand more complex Pi2s that do not necessarily fit into existing models, as outlined in this study.

[47] **Acknowledgments.** This work was supported by the NASA THEMIS project.

[48] Masaki Fujimoto thanks the reviewers for their assistance in evaluating this paper.

References

Angelopoulos, V. (2008), The THEMIS mission, *Space Sci. Rev.*, *141*, 5–34, doi:10.1007/s11214-008-9336-1.

Auster, H. U., et al. (2008), The THEMIS fluxgate magnetometer, *Space Sci. Rev.*, *141*, 235–264, doi:10.1007/s11214-008-9365-9.

Baumjohann, W., and K. H. Glassmeier (1984), The transient response mechanism and Pi2 pulsations at substorm onset: Review and outlook, *Planet. Space Sci.*, *32*, 1361–1370, doi:10.1016/0032-0633(84)90079-5.

Bester, M., M. Lewis, B. Roberts, J. McDonald, D. Pease, J. Thorsness, S. Frey, D. Cosgrove, and D. Rummel (2008), THEMIS operations, *Space Sci. Rev.*, *141*, 91–115, doi:10.1007/s11214-008-9456-7.

Bhattacharjee, A., Z. W. Ma, and X. Wang (1998), Ballooning instability of a thin current sheet in the high-Lundquist-number magnetotail, *Geophys. Res. Lett.*, *25*, 861–864, doi:10.1029/98GL00412.

Cheng, C. Z. (1991), A kinetic-magnetohydrodynamic model for low-frequency phenomena, *J. Geophys. Res.*, *96*, 21,159–21,171, doi:10.1029/91JA01981.

Cheng, C. Z., and A. T. Y. Lui (1998), Kinetic ballooning instability for substorm onset and current disruption observed by AMPTE/CCE, *Geophys. Res. Lett.*, *25*, 4091–4094, doi:10.1029/1998GL900093.

Elphinstone, R. D., et al. (1995), Observations in the vicinity of substorm onset: Implications for the substorm process, *J. Geophys. Res.*, *100*, 7937–7969, doi:10.1029/94JA02938.

Erickson, G. M., N. C. Maynard, W. J. Burke, G. R. Wilson, and M. A. Heinemann (2000), Electromagnetics of substorm onsets in the near-

geosynchronous plasma sheet, *J. Geophys. Res.*, *105*(A11), 25,265–25,290, doi:10.1029/1999JA000424.
Henderson, M. G. (2009), Observational evidence for an inside-out substorm onset scenario, *Ann. Geophys.*, *27*, 2129–2140, doi:10.5194/angeo-27-2129-2009.
Henderson, M. G., et al. (2006), Substorms during the 10–11 August sawtooth event, *J. Geophys. Res.*, *111*, A06206, doi:10.1029/2005JA011366.
Keiling, A., et al. (2006), Association of Pi2 pulsations and pulsed reconnection: Ground and Cluster observations in the tail lobe at 16 RE, *Ann. Geophys.*, *24*, 3433–3449, doi:10.5194/angeo-24-3433-2006.
Keiling, A., et al. (2008a), Periodic traveling compression regions during quiet geomagnetic conditions and their association with ground Pi2, *Ann. Geophys.*, *26*, 3341–3354, doi:10.5194/angeo-26-3341-2008.
Keiling, A., et al. (2008b), Correlation of substorm injections, auroral modulations, and ground Pi2, *Geophys. Res. Lett.*, *35*, L17S22, doi:10.1029/2008GL033969.
Keiling, A., et al. (2008c), Multiple intensifications inside the auroral bulge and their association with plasma sheet activities, *J. Geophys. Res.*, *113*, A12216, doi:10.1029/2008JA013383.
Kepko, L., M. G. Kivelson, and K. Yumoto (2001), Flow bursts, braking, and Pi2 pulsations, *J. Geophys. Res.*, *106*(A2), 1903–1915, doi:10.1029/2000JA000158.
Kim, K.-H., K. Takahashi, D.-H. Lee, P. R. Sutcliffe, and K. Yumoto (2005a), Pi2 pulsations associated with poleward boundary intensifications during the absence of substorms, *J. Geophys. Res.*, *110*, A01217, doi:10.1029/2004JA010780.
Kim, K.-H., D.-H. Lee, K. Takahashi, C. T. Russell, Y.-J. Moon, and K. Yumto (2005b), Pi2 pulsations observed from the Polar satellite outside the plasmasphere, *Geophys. Res. Lett.*, *32*, L18102, doi:10.1029/2005GL023872.
Lee, D. H. (1998), On the generation mechanism of Pi 2 pulsations in the magnetosphere, *Geophys. Res. Lett.*, *25*(5), 583–586, doi:10.1029/98GL50239.
Lee, D. H., and K. Kim (1999), Compressional MHD waves in the magnetosphere: A new approach, *J. Geophys. Res.*, *104*(A6), 12,379–12,385, doi:10.1029/1999JA900053.
Liang, J., et al. (2009), In-situ observation of ULF wave activities associated with substorm expansion phase onset and current disruption, *Ann. Geophys.*, *27*, 2191–2204, doi:10.5194/angeo-27-2191-2009.
Liou, K., C. I. Meng, P. T. Newell, K. Takahashi, S. I. Ohtani, A. T. Y. Liu, M. Brittnacher, and G. Parks (2000), Evaluation of low-latitude Pi2 pulsations as indicators of substorm onset using Polar ultraviolet imagery, *J. Geophys. Res.*, *105*, 2495–2502, doi:10.1029/1999JA900416.
Liu, W. W. (1997), Physics of the explosive growth phase: Ballooning instability revisited, *J. Geophys. Res.*, *102*, 4927–4931, doi:10.1029/96JA03561.
Lui, A. T. Y. (1996), Current disruption in the Earth's magnetosphere: Observations and models, *J. Geophys. Res.*, *101*, 13,067–13,088, doi:10.1029/96JA00079.
Lui, A. T. Y., and A.-H. Najmi (1997), Time-frequency decomposition of signals in a current disruption event, *Geophys. Res. Lett.*, *24*, 3157–3160, doi:10.1029/97GL03229.
Lui, A. T. Y., C.-L. Chang, A. Mankofsky, H.-K. Wong, and D. Winske (1991), A cross-field current instability for substorm expansions, *J. Geophys. Res.*, *96*(A7), 11,389–11,401, doi:10.1029/91JA00892.
Lyons, L. R., T. Nagai, G. T. Blanchard, J. C. Samson, T. Yamamoto, T. Mukai, A. Nishida, and S. Kokubun (1999), Association between Geotail plasma flows and auroral poleward boundary intensifications observed by CANOPUS photometers, *J. Geophys. Res.*, *104*, 4485–4500, doi:10.1029/1998JA900140.
McFadden, J. P., C. W. Carlson, D. Larson, V. Angelopoulos, M. Ludlam, R. Abiad, and B. Elliot (2008), The THEMIS ESA plasma instrument and in-flight calibration, *Space Sci. Rev.*, *141*, 277–302, doi:10.1007/s11214-008-9440-2.
Mende, S. B., S. E. Harris, H. U. Frey, V. Angelopoulos, C. T. Russell, E. Donovan, B. Jackel, M. Greffen, and L. M. Peticolas (2008), The THEMIS array of ground-based observatories for the study of auroral substorms, *Space Sci. Rev.*, *141*, 357–387, doi:10.1007/s11214-008-9380-x.
Miura, A. (2004), Validity of the fluid description of critical β and Alfvén time scale of ballooning instability onset in the near-Earth collisionless high-β plasma, *J. Geophys. Res.*, *109*, A02211, doi:10.1029/2003JA009924.
Miura, A., S. Ohtani, and T. Tamao (1989), Ballooning instability and structure of diamagnetic hydromagnetic waves in a model magnetosphere, *J. Geophys. Res.*, *94*(A11), 15,231–15,242, doi:10.1029/JA094iA11p15231.
Ohtani, S. (2001), Substorm trigger processes in the magnetotail: Recent observations and outstanding issues, *Space Sci. Rev.*, *95*, 347–359, doi:10.1023/A:1005231122496.
Ohtani, S., and T. Tamao (1993), Does the ballooning instability trigger substorms in the near-Earth magnetotail?, *J. Geophys. Res.*, *98*, 19,369–19,379, doi:10.1029/93JA01746.
Ohtani, S., K. Takahashi, L. J. Zanetti, T. A. Potemra, R. W. McEntire, and T. Iijima (1992), Initial signatures of magnetic field and energetic particle fluxes at tail reconfiguration: Explosive growth phase, *J. Geophys. Res.*, *97*, 19,311–19,324, doi:10.1029/92JA01832.
Pritchett, P. L., and F. V. Coroniti (1999), Drift ballooning mode in a kinetic model of the near-Earth plasma sheet, *J. Geophys. Res.*, *104*, 12,289–12,299, doi:10.1029/1999JA900092.
Raeder, J., D. Larson, W. Li, L. Kepko, and T. Fuller-Rowell (2008), Open GGCM simulations for the THEMIS mission, *Space Sci. Rev.*, *141*, 535–555, doi:10.1007/s11214-008-9421-5.
Roux, A., S. Perraut, P. Robert, A. Morane, A. Pedersen, A. Korth, G. Kremser, B. Aparicio, D. Rodgers, and R. Pellinen (1991), Plasma sheet instability related to the westward traveling surge, *J. Geophys. Res.*, *96*, 17,697–17,714, doi:10.1029/91JA01106.
Russell, C. T., P. J. Chi, D. J. Dearborn, Y. S. Ge, B. Kuo-Tiong, J. D. Means, D. R. Pierce, K. M. Rowe, and R. C. Snare (2008), THEMIS ground-based magnetometers, *Space Sci. Rev.*, *141*, 389–412, doi:10.1007/s11214-008-.
Saito, M. H., Y. Miyashita, M. Fujimoto, I. Shinohara,Y. Saito, K. Liou, and T. Mukai (2008), Ballooning mode waves prior to substorm-associated dipolarizations: Geotail observations, *Geophys. Res. Lett.*, *35*, L07103, doi:10.1029/2008GL033269.
Samson, J. C. (1985), Large-scale studies of Pi 2's associated with auroral breakups, *J. Geophys.*, *56*, 133–145.
Schindler, K., and N. F. Ness (1972), Internal structure of the geomagnetic neutral sheet, *J. Geophys. Res.*, *77*, 91–100, doi:10.1029/JA077i001p00091.
Sibeck, D. G., and V. Angelopoulos (2008), THEMIS science objectives and mission phases, *Space Sci. Rev.*, *141*, 35–59.
Solovyev, S. I., et al. (2000), Pi2 magnetic pulsation as response on spatio-temporal oscillations of auroral arc current system, *Geophys. Res. Lett.*, *27*, 1839–1842, doi:10.1029/2000GL000037.
Sutcliffe, P. R. (1998), Observations of Pi2 pulsations in a near ground state magnetosphere, *Geophys. Res. Lett.*, *25*, 4067–4070, doi:10.1029/1998GL900092.
Sutcliffe, P. R., and L. R. Lyons (2002), Association between quiet time Pi2 pulsations, poleward boundary intensification, and plasma sheet particle fluxes, *Geophys. Res. Lett.*, *29*(9), 1293, doi:10.1029/2001GL014430.
Takahashi, K., L. J. Zanetti, R. E. Lopez, R. W. McEntire, T. A. Potemra, and K. Yumoto (1987), Disruption of the magnetotail current sheet observed by AMPTE/CCE, *Geophys. Res. Lett.*, *14*(10), 1019–1022, doi:10.1029/GL014i010p01019.
Torr, M. R., et al. (1995), A far ultraviolet imager for the International Solar-Terrestrial Physics Mission, *Space Sci. Rev.*, *71*, 329–383.
Uozumi, T., et al. (2004), Propagation characteristics of Pi 2 magnetic pulsations observed at ground high-latitudes, *J. Geophys. Res.*, *109*, A08203, doi:10.1029/2003JA009898.
Voronkov, I. O., E. F. Donovan, and J. C. Samson (2003), Observations of the phases of the substorm, *J. Geophys. Res.*, *108*(A2), 1073, doi:10.1029/2002JA009314.
Webster, D. J., J. C. Samson, and G. Rostoker (1989), Eastward propagation of transient field-aligned currents and Pi2 pulsations at auroral latitudes, *J. Geophys. Res.*, *94*, 3619–3630, doi:10.1029/JA094iA04p03619.
Yumoto, K., et al. (1996), The STEP 210° magnetic meridian network project, *J. Geomagn. Geoelectr.*, *48*, 1297–1309, doi:10.5636/jgg.48.1297.

A. Keiling, Space Sciences Laboratory, University of California, Berkeley, CA 94720, USA. (keiling@ssl.berkeley.edu)